JGR Atmospheres

RESEARCH ARTICLE
10.1029/2020JD034525

Special Section:
Carbon Weather: Toward the next generation of regional greenhouse gas inversion systems

Seasonal Variability in Local Carbon Dioxide Biomass Burning Sources Over Central and Eastern US Using Airborne In Situ Enhancement Ratios

Joshua P. DiGangi[1], Yonghoon Choi[1,2], John B. Nowak[1], Hannah S. Halliday[1,3,4], Glenn S. Diskin[1], Sha Feng[5,6], Zachary R. Barkley[5], Thomas Lauvaux[5,7], Sandip Pal[8], Kenneth J. Davis[5], Bianca C. Baier[9,10], and Colm Sweeney[10]

[1]NASA Langley Research Center, Hampton, VA, USA, [2]Science Systems and Applications, Inc., Hampton, VA, USA, [3]Universities Space Research Association, Columbia, MD, USA, [4]Now at: US EPA Research Triangle Park, Durham, NC, USA, [5]The Pennsylvania State University, University Park, PA, USA, [6]Now at: Atmospheric Sciences and Global Change Division, Pacific Northwest National Laboratory, Richland, WA, USA, [7]Now at: LSCE/IPSL, Gif sur Yvette, France, [8]Department of Geosciences, Atmospheric Science Division, Texas Tech University, Lubbock, TX, USA, [9]Cooperative Institute for Research in Environmental Sciences, University of Colorado-Boulder, Boulder, CO, USA, [10]NOAA Global Monitoring Laboratory, Boulder, CO, USA

Key Points:

- Airborne CO and CO_2 enhancement ratios used to examine distribution of CO_2 emissions by combustion source efficiency
- Discrepancies observed between model and airborne results in seasonal and regional behavior of biomass: fossil fuel burning CO_2 emission ratios
- Satellite fire data suggest discrepancies may be partially due to mix of spatial resolution and biomass/fire parameterization

Supporting Information:

Supporting Information may be found in the online version of this article.

Correspondence to:

J. P. DiGangi,
joshua.p.digangi@nasa.gov

Citation:

DiGangi, J. P., Choi, Y., Nowak, J. B., Halliday, H. S., Diskin, G. S., Feng, S., et al. (2021). Seasonal variability in local carbon dioxide biomass burning sources over central and eastern US using airborne in situ enhancement ratios. *Journal of Geophysical Research: Atmospheres*, *126*, e2020JD034525. https://doi.org/10.1029/2020JD034525

Received 31 DEC 2020
Accepted 3 NOV 2021

Abstract We present observations of local enhancements in carbon dioxide (CO_2) from local emissions sources over three eastern US regions during four deployments of the Atmospheric Carbon Transport-America (ACT-America) campaign between summer 2016 and spring 2018. Local CO_2 emissions were characterized by carbon monoxide (CO) to CO_2 enhancement ratios (i.e., $\Delta CO/\Delta CO_2$) in air mass mixing observed during aircraft transects within the planetary boundary layer. By analyzing regional-scale variability of CO_2 enhancements as a function of $\Delta CO/\Delta CO_2$ enhancement ratios, observed relative contributions to CO_2 emissions were separated into fossil fuel and biomass burning (BB) regimes across regions and seasons. CO_2 emission contributions attributed to biomass burning ($\Delta CO/\Delta CO_2 > 4\%$) were negligible during summer and fall in all regions but climbed to ~9%–11% of observed combustion contributions in the South during winter and spring. Relative CO_2 fire emission trends matched observed winter and spring BB contributions, but conflictingly predicted similar levels of BB during the fall. Satellite fire data from MODIS and VIIRS suggested the use of higher spatial resolution fire data that might improve modeled BB emissions but were not able to explain the bulk of the discrepancy.

1. Introduction

Carbon dioxide (CO_2) is a primary product of combustion and a relatively inert compound in the atmosphere, and total CO_2 emissions collectively have a strong influence on global climate. Thus, accurately quantifying the accumulation of atmospheric CO_2 from its broad variety of sources is critical to predicting future trends in global temperature and climate. Models utilize emission inventories of CO_2, combined with ocean and land biosphere models, to make predictions of future climate (Fyfe et al., 2021; Gregory et al., 2009). Thus, the proper apportionment and quantification of emission sources is important for models to accurately update how emissions change over time. For CO_2, fossil fuel combustion is one of the primary global anthropogenic sources, but sources range widely in terms of both spatial distribution and emission type (Gurney et al., 2020a). In particular, biomass burning (BB) remains a difficult source to constrain due to its unpredictable timing and wide variety of vegetative fuels and burning conditions. As a result, emission inventories must be regularly evaluated through observations, either through direct comparison with flux measurements (Hannun et al., 2020; Jung et al., 2011) or more typically, concentration measurements in conjunction with inversion models (Cui et al., 2021; Lauvaux et al., 2012; Wang et al., 2018). Tower networks enable vital long term, continuous, high accuracy records of CO_2 levels, but are limited in spatial coverage. Satellite measurements provide global coverage, but with limited spatial and temporal resolution as well as limited comparability with in situ measurements (Eldering et al., 2017; Yokota et al., 2009). Airborne measurements of CO_2 bridge these two spatial regimes, providing data with high spatial resolution and comparability over a broad area, making them well suited for regional emission surveys.

Carbon monoxide (CO) is a ubiquitous carbon oxidation intermediate with an atmospheric lifetime on the order of weeks to months and is the chemical precursor to gas-phase CO_2 formation (Holloway et al., 2000). While the

Table 1
ACT-America Flight Dates by Season and Nominal Region

Campaign	Sampling dates		
	Mid-Atlantic	Midwest	South
Summer 2016	18 July to 1 August	1–16 August	16–29 August
Winter 2017	27 February to 10 March	13–27 February	30 January to 13 February
Fall 2017	3–16 October	16–30 October	30 October to 13 November
Spring 2018	4–20 May	23 April to 8 May	12–23 April

primary source of CO is through combustion, other sources can include direct biological emission and oxidation of volatile organic compounds (VOCs) (Griffin et al., 2007). Enhancement ratios of CO vs CO_2 ($\Delta CO/\Delta CO_2$) can be particularly powerful for evaluating combustion sources, as the ratio of a plume from a single point source provides information about the source's combustion efficiency (CE). High efficiency (fuel-lean, high temperature) combustion produces relatively little CO, as the fuel carbon is nearly completely converted to CO_2. Low efficiency (fuel-rich, lower temperature) combustion converts less of the fuel carbon to CO_2, resulting in the release of greater amounts of intermediate combustion products, such as CO and organic compounds. For example, vehicular emissions in the United States typically have emission ratios in the range of <2% $\Delta CO/\Delta CO_2$ (Djuricin et al., 2010; Graven et al., 2009; LaFranchi et al., 2013; Turnbull et al., 2011), whereas modern power plant emissions typically are much more efficient, less than <0.1% $\Delta CO/\Delta CO_2$ (Peischl et al., 2010; USEPA, 2010). BB emissions typically have emission ratios on the order of 4% or higher $\Delta CO/\Delta CO_2$ (Akagi et al., 2011; Andreae & Merlet, 2001; Suntharalingam et al., 2004), which makes $\Delta CO/\Delta CO_2$ enhancement ratios a reliable marker for distinguishing uncontrolled BB from controlled fossil fuel (FF) combustion.

The recent NASA Atmospheric Carbon Transport-America (ACT-America) airborne study provides an ideal test case to examine trends in CO_2 sources over central and eastern United States and to compare them to model-derived seasonal and regional trends. In particular, the high-resolution, concurrent measurements of CO and CO_2 allow for a bottom-up perspective of the influence of various combustion sources on CO_2 emissions with respect to the inferred CE, allowing for apportionment between BB and FF emissions. We present a technique similar to that reported by Halliday et al. (2019), which utilized distributions of $\Delta CO/\Delta CO_2$ determined using a rolling background to examine relative combustion regime contributions and sources, expanding the method in order to ascertain contributions to local CO_2 emissions. The aim is to examine the seasonal and regional variability in CO_2 emissions over three regions in the eastern and central US using aircraft measurements obtained within the seasonal ACT-America field campaigns. These results are then compared to spatially and temporally concurrent modeled BB CO_2 emission products, as well as the satellite fire products that drive those emissions, in order to evaluate the model emissions response with respect to season and region in the eastern half of the United States.

2. Materials and Methods

2.1. ACT-America

The ACT-America campaign was a NASA Earth Venture Suborbital project focused on reducing errors in inversion models of the transport and emissions of atmospheric carbon dioxide and methane over the continental United States (Davis et al., 2021; Wei et al., 2021). ACT-America consisted of seasonal six-week intensives with three deployments per intensive; sampling locations and dates are shown in Table 1. Each deployment is sampled over three separate regions as shown in Figure 1. Measurements were collected using two aircraft: the NASA Wallops Flight Facility C-130 (N436NA) and the NASA Langley Research Center B-200 King Air (N529NA). The C-130 was instrumented with in situ chemistry measurements (Kostinek et al., 2019), whole air sampling (Baier et al., 2020), and remote sensing measurements (Campbell et al., 2020; Pal et al., 2020). The B-200 was instrumented with in situ measurements (Weibring et al., 2020) and whole air sampling measurements. The two aircraft combined to collect a mixture of planetary boundary layer (PBL) as well as lower and upper free tropospheric data. Three types of flight patterns were flown: frontal passage flights aimed at describing the transport of greenhouse gases (GHGs) by midlatitude cyclones (Pal et al., 2020), fair weather flights aimed at constraining regional fluxes, and OCO-2 validation flights aimed at quantifying CO_2 levels over multiple altitudes under an

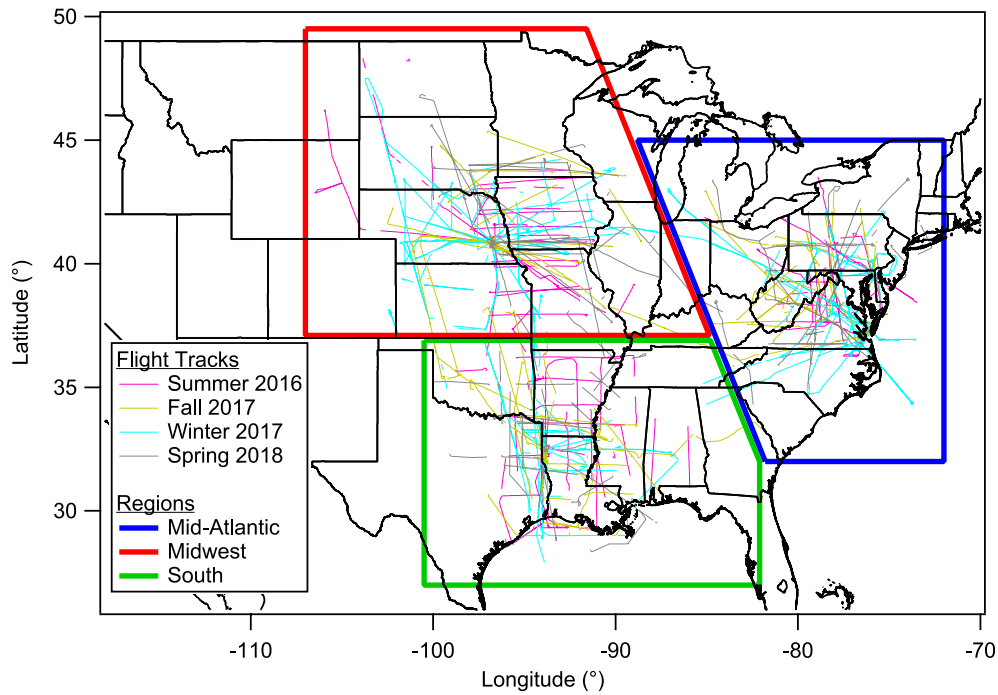

Figure 1. Map of ACT-America flight domains. All flight tracks at <1 km AGL for each season. Colored boxes denote the regions defined in this study. The border between the Midwest and South regions was 37°N, while the border between the Mid-Atlantic region and the other two was a line drawn between 45°N, 89°W and 32°N, 82°W.

OCO-2 satellite track (Bell et al., 2020). Flight patterns primarily focused on level altitude legs at either 300 m above ground level (AGL) for PBL measurements or constant pressure altitude flight levels above the PBL ranging up to 9 km MSL. Flights were conducted primarily in midday conditions. While flights were at times conducted in areas with broad, regional plumes, individual sources were not targeted.

2.2. In Situ Airborne Measurements

The two aircraft contained identical payloads for measuring in situ gas phase carbon species as described in Wei et al. (2021) and summarized here in brief. CO_2, CO, and methane (CH_4) dry mole fractions were measured using a commercial cavity ringdown spectrometer (G2401-m, PICARRO, Inc.) with a custom gas sampling and calibration system (Figure S1 in Supporting Information S1). The spectrometer cycled between measurements of each species sequentially every 2.5 s. The instrument temporal response through the gas system and instrument was measured to be typically ∼2–3 s. The calibration gas was humidified to the same level as the dried ambient sample air (typically 0.03%–0.05%), thus avoiding water vapor-dependent calibration discrepancies (Reum et al., 2019). Single concentration calibrations were performed hourly during flight to assess instrument offsets. Linear slope calibrations were conducted weekly on the ground through three-point calibrations over a broader concentration range. All calibration gases were traceable to the CO_2 X2007 (Tans et al., 2017), CO X2014A (Novelli et al., 1991), and CH_4 X2004A (Dlugokencky et al., 2005) WMO scales (NOAA ESRL). Inflight wing-tip-to-wingtip in situ comparisons as well as in-flight in situ/flask comparisons (Baier et al., 2020), all agreed within experimental error. Measurement precision was 0.1 ppm, 5 ppb, and 1 ppb in 2.5 s for CO_2, CO, and CH_4, respectively. Measurement accuracy was 0.1 ppm, 2%, and 1 ppb for CO_2, CO, and CH_4, respectively.

2.3. Airborne $\Delta CO/\Delta CO_2$ Analysis

$\Delta CO/\Delta CO_2$ were derived using a short-term sliding slope window (Halliday et al., 2019; Smith et al., 2015). Using a sliding fixed-time bin window over the CO and CO_2 time series measured at ∼2.5 s intervals and binned at 5 s intervals, a linear regression of CO vs CO_2 is calculated for each period. This results in a linear slope equivalent to $\Delta CO/\Delta CO_2$ and a coefficient of determination (r^2) for each bin, where r^2 can then be used to filter

uncorrelated bins that do not represent identifiable mixing. The resulting values can then be displayed as a distribution of slopes representative of the mixing observed over certain regions and/or timescales.

For this work, running-bin linear regressions of $\Delta CO/\Delta CO_2$ were calculated using weighted orthogonal distance regression (ODRPACK95 - IGOR Pro v7), which Wu and Yu (2018) found to return equivalent unbiased slopes compared to the York regression used by Halliday et al. (2019). For each fit, CO and CO_2 mole fractions were weighted by the measurement precisions of 0.1 ppm for CO_2 and 5 ppb for CO. In order to focus on the relative enhancement ratios of local sources in the PBL, all data above 1 km AGL were rejected in order to focus on the 300 m level altitude flight legs. Values of $\Delta CO/\Delta CO_2$ were calculated using data from the ACT-America 5 s merge (Davis et al., 2018).

This resulted in binned frequency distributions of $\Delta CO/\Delta CO_2$ enhancement ratio slopes at 0.1% resolution. In Halliday et al. (2019), while the raw frequency distribution depended heavily on the choice of r^2 cutoff and bin window size, the normalized distribution was insensitive to both factors. To estimate the variability due to these factors, sensitivity tests were performed for each parameter over a range of r^2 values (0.3, 0.4, 0.5, 0.6, 0.7, and 0.8) and bin windows (30, 45, 60, 90, and 120 s), for a total of 30 different values. Figures S2–S5 in Supporting Information S1 shows line histograms of the distribution of $\Delta CO/\Delta CO_2$ observed during the four campaigns. The results were similar to those observed by Halliday et al. (2019) in that there was wide variability in the raw frequency distribution intensities, but very similar normalized frequencies regardless of parameter value.

To examine the relationship between CO_2 and CE, an extension of the technique is required. Thus, each observed slope was binned by both $\Delta CO/\Delta CO_2$ and the total ΔCO_2 in the bin, the latter used as a metric for the CO_2 intensity of the emission. The result is a 2D heat map representing the enhancement in CO_2 as a function of $\Delta CO/\Delta CO_2$ enhancement ratio (Figure 2a). To calculate the ΔCO_2-weighted distribution with respect to $\Delta CO/\Delta CO_2$, the data were summed with respect to ΔCO_2 for each $\Delta CO/\Delta CO_2$ bin:

$$\mathrm{NWF}\left(\left(\frac{\Delta CO}{\Delta CO_2}\right)_j\right) = 100\% * \frac{\sum_i n_{i,j} * \Delta CO_{2,i}\left(\left(\frac{\Delta CO}{\Delta CO_2}\right)_j\right)}{\sum_j \sum_i n_{i,j} * \Delta CO_{2,i}\left(\left(\frac{\Delta CO}{\Delta CO_2}\right)_j\right)} \tag{1}$$

where NWF is the normalized ΔCO_2-weighted bin frequency as a function of $\Delta CO/\Delta CO_2$, while $n_{i,j}$ is the number of points in the ith bin of ΔCO_2 and the jth bin of $\Delta CO/\Delta CO_2$. Thus, NWF represents the relative contribution toward CO_2 emissions of a given $\Delta CO/\Delta CO_2$ enhancement ratio, and integrated NWF values over a range of $\Delta CO/\Delta CO_2$ enhancement ratios represent the relative contribution in CO_2 emissions from the CE source represented by that range. Figures 2b and 2c shows the resultant NWF distribution for the measurements collected during the spring campaign at less than 1 km altitude. The same sensitivity analyses to r^2 and bin width were performed as with the unweighted normalized method. NWF values were similarly insensitive to the choice of r^2 cutoff and bin size (Figures S6–S9 in Supporting Information S1), though with somewhat more variability than the unweighted method. Thus, the final NWF value was calculated as the average of the 30 values from the sensitivity analyses over the different combinations of r^2 and bin width parameters listed above, with the gray shaded areas in Figures 2b and 2c showing the full variability from these different cutoff choices. Instrument error was neglected for the NWF analysis (other than in the fits), as it is a relatively small contribution compared to the cutoff error (Halliday et al., 2019).

One of the key advantages of this technique is that, by focusing on $\Delta CO/\Delta CO_2$ slopes, it does not rely on broad regional assumptions about homogeneous background levels of CO and CO_2. CO and CO_2 background mole fractions are calculated on a bin-sized time frame (i.e., 30–120 s). The aircraft ground speed was typically from 100–120 m/s at these altitudes, thus the spatial extent of the bin windows varied between 3 and 14 km. This smaller background scale results in more robust enhancement factors that do not experience the background error biases of a regional background method, as any background variability on spatial scales greater than 14 km would have no influence on the calculated enhancement factors. Additionally, as the NWF distributions were not strongly dependent on bin window size, any biases in calculated enhancement factors due to background variability between 3 and 14 km are captured by the NWF error. As a result, this method is rigorous to any changes in background on scales >3 km, though it is still subject to variability on smaller scales.

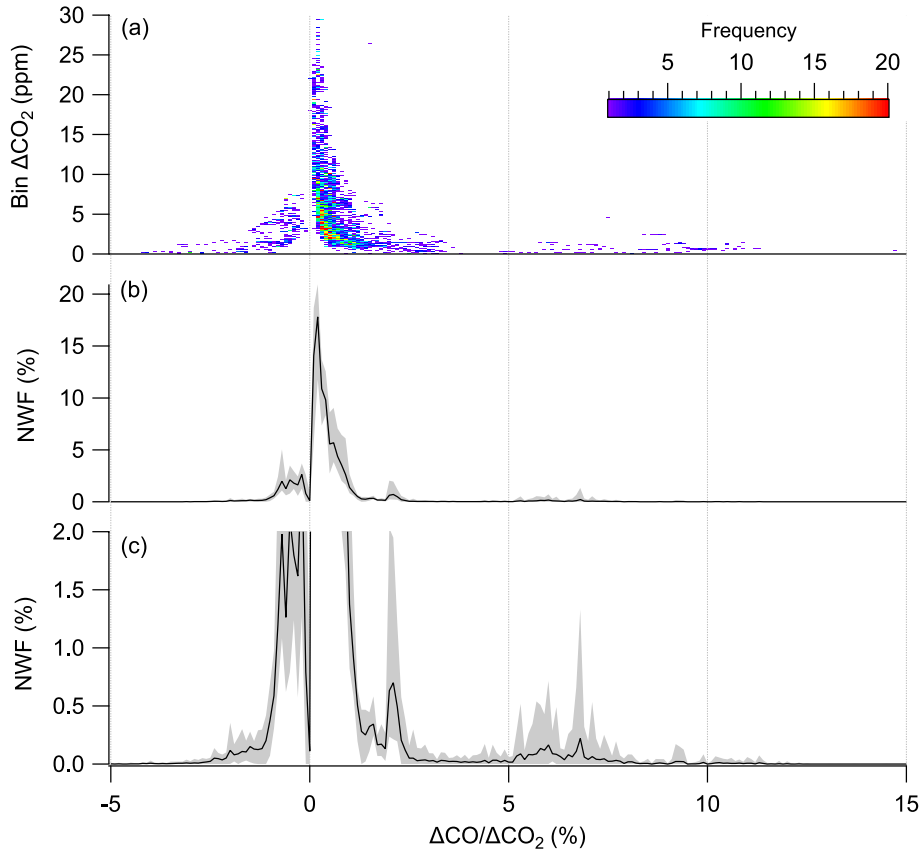

Figure 2. (a) Example heat map of plume frequency binned by ΔCO_2 and by $\Delta CO/\Delta CO_2$ slope from the spring 2018 deployment with 0.6 r^2 cutoff and a 60 s rolling bin window. (b) Normalized ΔCO_2-weighted frequency (NWF) distributions of CO_2 contributions with respect to $\Delta CO/\Delta CO_2$ enhancement ratios averaged over all r^2 cutoffs and bin sizes from spring 2018 deployment. Gray shaded areas denote full range in variability in NWF values across all r^2 cutoffs and bin sizes. (c) Same as (b), but vertically enhanced to highlight BB influence at $\Delta CO/\Delta CO_2 > 4\%$.

Another important caveat of the technique is that very high CE sources with very low $\Delta CO/\Delta CO_2$ emission ratios (e.g., power generation plants; Peischl et al., 2010; USEPA, 2010) could be missed if the measured enhancements were below the instrument precision. In addition, this technique does not describe the total amount of CO_2 emissions, only the relative contributions nearby point sources with different enhancement ratios from the background. Thus, the technique is internally consistent across seasons, well suited at looking at relative differences in contributions from different CE sources, but not a good predictor of absolute CO_2 emissions from BB and FF combustion. A near-field source would be observed as a stronger contribution than a more distant source, making the method more biased toward near-field sources. This should be somewhat mitigated by the tendency for more distant plumes to have broadened signatures, which would translate to a greater count frequency, albeit weaker, provided it has a significantly different ratio from the background. This mitigation should be less effective at higher bin widths, which may account for some of the greater variability in the ΔCO_2-weighted NWF compared to the unweighted normalized frequency. This same effect makes it impossible to define an exact receptor footprint for the results other than this weighting effect on source distance.

2.4. Modeled BB CO_2 Emissions

Modeled CO_2 fire flux components were obtained from NOAA's CarbonTracker: version CT2017 (CarbonTracker Team, 2018) for the summer 2016 campaign and CT-Near Real Time (NRT).v2019-2 release (Peters et al., 2007) for the other 3 seasons. The fire module in both CT2017 and CT-NRT.v2019-2 models pyrogenic CO_2 emissions using the GFED4.1s and GEFD_CMS fire module (Giglio et al., 2013; van der Werf et al., 2017), which uses MODIS 1° fire products to detect fires and the CASA model to convert burned area to a CO_2 flux.

Fire emission fluxes were calculated from the average of the outputs of the GFED4.1s and GEFD_CMS modules with 3 h time resolution and 1° latitude by 1° longitude spatial resolution over the same dates and years as the observations. To enhance the near-field comparison with the observed data, fire fluxes were subsampled to a 27 km^2 grid, roughly double the 14 km maximum bin window spatial extent of the $\Delta CO/\Delta CO_2$ NWF analysis. Regional uncertainty was estimated to be ~50%, with possibly higher values in regions with a high prevalence of smaller fires (van der Werf et al., 2017).

2.5. Modeled FF CO_2 Emissions

Modeled FF CO_2 emissions were calculated using the Vulcan v3.0 emissions inventory (Gurney et al., 2020a). The Vulcan inventory provides hourly CO_2 emissions at 1 km^2 resolution for the years 2010–2015 (Gurney et al., 2020b). CO_2 emissions are separated into 10 sectors: onroad (vehicles), electricity production, residential, nonroad (off-road vehicles), airport, commercial, industrial, commercial marine vehicles, rail, and cement. Emission data were sourced from various inventories, primarily the US Environmental Protection Agency National Emission Inventory. For comparison with the modeled fire emissions in this analysis, the 2015 hourly 1 km^2 Vulcan emissions were averaged spatially to the same 27 km^2 grid as the fire emissions. Cement sources were not included in the analysis, as the carbonate decomposition process that produces the majority of CO_2 emissions does not result in strong coemissions of CO (Andrew, 2018). Vulcan emissions were also averaged temporally between 0900 and 1700 local time to align with the aircraft flight times and minimize any biasing effects of the diurnal cycle of CO_2 emissions (Turnbull et al., 2015).

3. Results

3.1. Seasonal $\Delta CO/\Delta CO_2$ Variability

NWF is weighted by the magnitude of the enhancement in CO_2, and thus changes in the NWF distribution across various $\Delta CO/\Delta CO_2$ enhancement ratios can be used to evaluate the relative contributions of those CO_2 emission sources and their inferred CE. In this analysis, we classified the NWF distributions into regimes with respect to enhancement factor and use the variability between these regimes to infer the relative strength of the CO_2 combustion sources. Figure 3 shows the total integrated NWF contributions vs $\Delta CO/\Delta CO_2$ slope distribution for each deployment during different seasons, while Table S1 in Supporting Information S1 shows the numerical integrated NWF contributions in each regime.

Regimes were delineated by the natural minima in the NWF distributions. Common minima over all seasons exist at $\Delta CO/\Delta CO_2$ enhancement factors of 0% and ~4%. The 0% minimum is a result of the technique, as enhancement ratios of 0% would have a low correlation. The 4% minimum is consistent with the lower end of reported biomass burning CE (Akagi et al., 2011; Andreae & Merlet, 2001; Suntharalingam et al., 2004). As a result, the FF regime is defined as $\Delta CO/\Delta CO_2$ enhancement ratios between 0% and 4%, and the BB regime is defined as enhancement ratios greater than 4%. A third regime consists of enhancement ratios with negative slopes (NS regime) or $\Delta CO/\Delta CO_2$ less than 0%. Since a negative enhancement ratio cannot be explained in the context of combustion efficiency, its existence implies a more complex mixing process likely influenced by CO_2 biogenic uptake as non-photochemical CO sinks are not known to be common. In particular, these negative enhancement ratios have been hypothesized to be associated with ecosystem uptake (Halliday et al., 2019; Silva et al., 2013) with either a photochemical or a well-mixed anthropogenic CO source. The implications of the NS regime are further discussed in Section 4.1. Efficient controlled combustion of non-fossil fuels (e.g., high-temperature wood fired furnace) could result in lower enhancement ratios akin to those typically expected for FF (Venkataraman & Rao, 2001), while inefficient combustion of FF (e.g., uncontrolled open oil burning) could result in higher enhancement ratios akin to those expected from BB (Middlebrook et al., 2012). These sources are relatively rare compared with the ubiquity of typical FF and BB combustion and thus will be neglected for the purposes of this analysis.

NWF contributions from NS regime peaked during the summer campaign, exhibited smaller contributions in spring and fall, respectively, and were negligible in winter. This pattern is consistent with the expected CO_2 biogenic processing behavior in each season. FF regime contributions were consistently the majority in all seasons, though relatively more prevalent during the fall due to the lack of BB regime contributions and lower NS contributions compared to summer. While in summer, enhancement ratios within the FF regime were predominantly

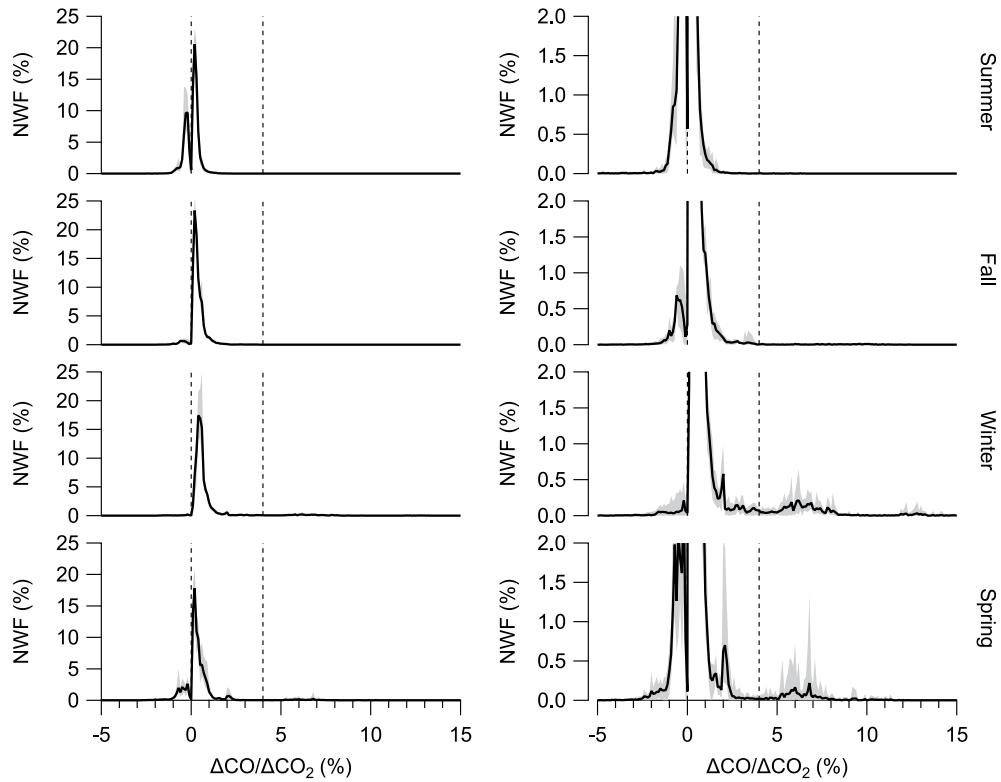

Figure 3. NWF distributions as a function of $\Delta CO/\Delta CO_2$ for PBL (<1 km AGL) for each season. Left panels show the full scale of the NWF distribution, while right panels show a vertically enhanced scale of NWF values <2% to highlight contributions to the BB regime. The solid black line denotes the average NWF from the r^2 and bin size sensitivity tests while the gray shading shows the full extent of the NWF values from these sensitivity tests.

between 0% and 1%, while NWF contributions at enhancement ratios between 1% and 4% became much more significant particularly in the winter and spring. It remains uncertain whether this is a real variability from differing seasonal FF CE, but it is likely influenced by biogenic CO_2 uptake.

BB regime NWF contributions were observed to be very weak in the summer and fall but were ~4% and ~2.5% of observed NWF in winter and spring, respectively. This finding is consistent with visual observations of BB during the campaign, as agricultural fires were observed to be common especially during the winter campaign. The primary BB regime peaks at enhancement ratios between 5% and 8%, in both winter and spring and is indicative of higher CE flaming BB (Andreae & Merlet, 2001). However, weaker peaks at higher enhancement ratios were observed between 10%–14% in winter and 9%–12% in spring, indicating the additional presence of smoldering and/or mixed phase sources.

3.2. Regional $\Delta CO/\Delta CO_2$ Variability

Observed enhancement ratios were also segregated into three ACT-America flight domains: Mid-Atlantic, Midwest, and South (Figure 1) to examine how well the calculated CE aligns with ACT-America observations and our current knowledge of activities in these three regions. Figure 4 shows the relative seasonal NWF contributions for each regime within the PBL both in total and for each region. In summer, the strong NWF contributions in the NS regime (Figure 4c) are primarily driven by observations in the Mid-Atlantic and Midwest regions, with South region NS contributions only about 25% of that of the other regions. This general trend is consistent with previously reported regional trends in measurements from the Orbiting Carbon Observatory (OCO-2) of solar-induced fluorescence (SIF). Sun et al. (2018) discussed averaged SIF retrievals for June-August 2015 and higher SIF levels were observed over the East and Midwest regions compared to the South. As SIF has been shown to be correlated with gross primary production (Sun et al., 2018), which is related to the rate of bio-

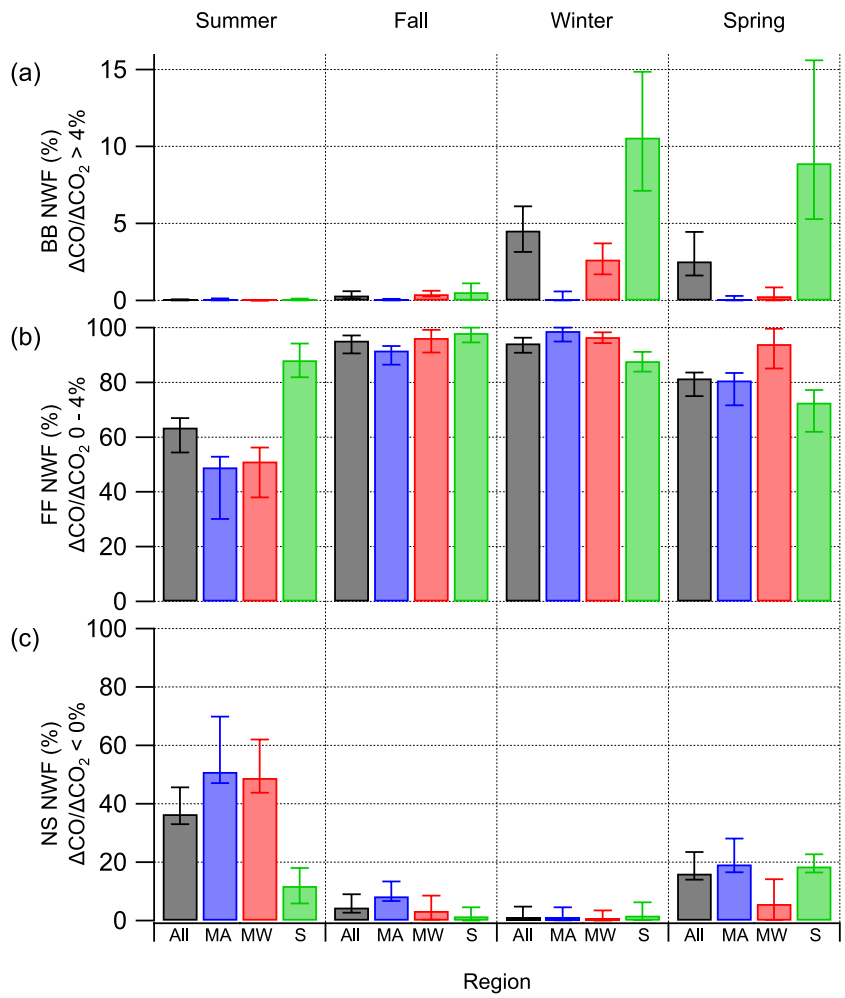

Figure 4. NWF contributions separated by season and region (MA-Mid-Atlantic, MW-Midwest, and S-South) measured in the PBL (<1 km AGL) for the (a) BB, (b) FF, and (c) NS regimes. Error bars denote range in variability in the r^2 and bin size sensitivity analyses.

sphere carbon fixation, higher SIF levels imply greater biospheric CO_2 uptake. This is further evidence, albeit circumstantial, of the relationship between the NS regime and biogenic uptake. Southern region NS contributions were at their highest during spring, possibly due to the earlier start to the agricultural growing season. Fall and winter NS contributions were much smaller than the other seasons in all regions, with <10% average NWF contributions.

In the BB NWF regime (Figure 4a), the Southern region dominates the enhanced contributions observed during the winter ($10.5^{+4.3}_{-3.5}$% NWF) and spring ($8.9^{+6.7}_{-3.6}$% NWF), the seasons having similar contributions with a winter to spring ratio of $1.27^{+0.78}_{-0.68}$. Mid-Atlantic region BB contributions were negligible over all seasons. Midwestern region BB contributions were only significant during the winter and fall, with a winter to fall ratio of $6.5^{+2.0}_{-3.0}$. However, during winter, the Midwestern BB contributions were still much smaller than those from the Southern region, with a winter South to Midwest ratio of $4.05^{+0.98}_{-0.68}$. During fall, winter, and spring, FF NWF regime contributions were similar across all regions but were weaker during summer in the Mid-Atlantic and Midwest compared to in the South, corresponding to the weaker NS regime contributions observed in the South during summer.

4. Discussion

4.1. Biogenic Uptake and the NS Regime

Biogenic uptake can affect the calculation of the $\Delta CO/\Delta CO_2$ enhancement ratios in several ways. For instance, if the CO_2 background fluctuates due to uptake on the scale of the bin window, then these fluctuations would bias the fit slope potentially both positively and negatively, as well as reducing the goodness of fit. The agreement of NWF in the sensitivity analysis with respect to bin window size, equating to a range of 3–14 km, provides confidence that this variable was not a strong factor in the results, and the net effects of any CO_2 background variability within this range would be represented by the NWF uncertainty. Variability below 3 km could still affect the analysis, but those scales approach the size of the PBL during ACT-America (typically 1–2 km; Gonzalez et al., 2021), likely resulting in any variability at those small scales to be well-mixed. Thus, this form of the influence of biogenic uptake of CO_2 is not expected to be a significant influence on enhancement ratios in this analysis. Additionally, oxidation of biogenic volatile organic compounds (VOCs) can lead to significant CO production. As biogenic VOC emissions should correlate with biogenic CO_2 uptake, this would result in increased observations of negatively sloped enhancement ratios. Gonzalez et al. (2021) found that in an analysis of North American summer CO sources, including the ACT-America domains, the combination of biogenic VOC oxidation and fire CO sources represented a plurality (40%–45%) of above background enhancements in CO compared to only 9%–16% from FF sources. This contrasted with other seasons where FF remained the largest regional CO source. This trend circumstantially agrees with the strong NS NWF contribution observed during the summer compared to other seasons, in which case it would be expected that the enhancements in the NS regime are independent of the FF regime.

Another effect involves the mixing of air with different biogenic uptake history. For example, if an air mass with a well-mixed combination of biogenic CO_2 uptake and FF emissions mixes with a clean air mass with less biogenic CO_2 uptake, the difference in CO_2 due to the uptake signature could artificially increase the observed enhancement ratio of the FF source compared to its actual CE. If the cleaner source experienced more biogenic uptake than the FF-influenced source, the apparent enhancement ratio would be artificially decreased compared to the FF source's CE. This explanation is also consistent with the seasonal trend in the NS regime but has different implications. Unlike the biogenic VOC oxidation theory, the mixing theory would affect both positive and negative enhancement ratios. It also provides insight into what extent this bias may play in the results of this analysis. In Figure 3, the NS regime NWF contributions are at $\Delta CO/\Delta CO_2$ slopes $> -1\%$, which suggests that the extent of this effect is likely to shift enhancement ratios no more than 1%–2%. Combined with the distinct distribution of the BB NWF contributions at $\Delta CO/\Delta CO_2$ slopes >4% vs. the FF regime, we can infer that any bias predominantly affects our calculation of the FF regime. While the enhancement ratios of the BB regime may still be affected by this form of bias, the distinct BB regime distribution would negate this effect on the integrated BB regime contribution.

The BB regime can still be affected indirectly in terms of relative intensity. Since our analysis technique yields relative distributions, any bias in the FF regime would change the scale of the total signal in the BB regime. Thus, a sensitivity test using the NS regime data can help constrain some of this FF regime bias that we observe. For this test, we examined three cases. The base case involved normalizing the integrated BB regime by the integrated FF regime, neglecting the NS regime. This case represents one in which the NS regime was exclusively driven by observations of biogenic VOC oxidation-sourced CO plumes combined with CO_2 biogenic uptake, where mixing with these two regimes would have no effect on the positive enhancement ratios. The second case involved normalizing the BB regime by the sum of the FF and NS regimes. This case represents an NS regime entirely driven by FF emissions that were shifted toward negative slopes by the changes in biogenic background. The third case involved normalizing the BB regime by the difference between the FF and NS regimes. This case represents an NS regime driven by mixing, but one where this affected the negative slopes and positive slopes equally. In other words, the combined mixing and biogenic uptake would create an equal bias in both the positive and negative sloped regimes. All of these cases are meant to be extremes, which can be used to constrain the potential influence on the BB regime.

For each of these cases, the normalized BB regime was calculated for each of the same 30 combinations of r^2 and bin window settings as discussed in Section 2.3. Figure 5 shows the results of this sensitivity test. Despite summer having the largest contributions to the NS regime, the BB/FF ratio for all cases in each region remained

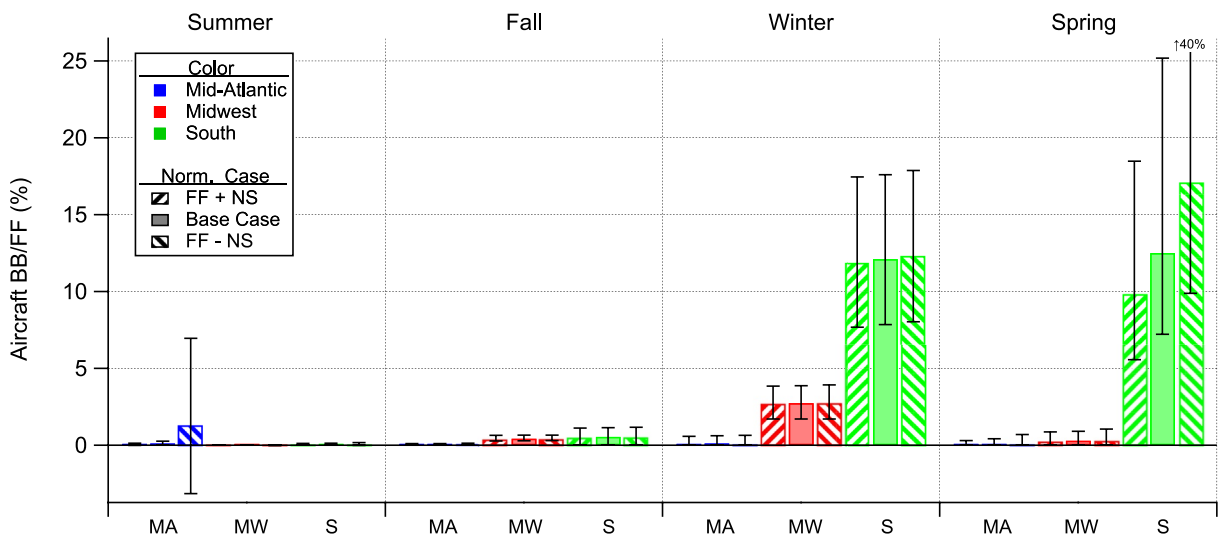

Figure 5. Sensitivity analysis of the ratio of the FF-normalized BB NWF contributions separated by season and region (MA-Mid-Atlantic, MW-Midwest, and S-South). Patterns indicate sensitivity case, where "FF–NS" is normalization by difference between the FF and NS regime contributions, "base case" is normalization by just the FF regime, and "FF + NS" is normalization by the sum of the FF and NS regime contributions. Error bars denote range in variability from r^2 and bin window sensitivity analysis.

negligible due to the small BB regime contributions. One exception was in the South, where BB was normalized by the difference between the FF and NS regimes. In this case, for some combinations of r^2 and bin width, the NS regime contributions were larger than those from the FF regime, resulting in a prediction of negative BB/FF. As it is unlikely that no signatures of FF combustion were detected, combined with the lack of absolute detections of BB enhancement ratios, this appears to be a statistical artifact of this worst-case scenario. During fall and winter, the difference between the three cases is minimal, as NS regime contributions were low during both seasons. In contrast, the spring season had the largest variability between cases due to the combined high BB regime contributions in the South and significant NS regime contributions. Overall, the systematic trends between regions and seasons stand over all cases. As the base case uncertainty encompasses the majority of the variability within the other two extreme cases, the remaining discussion will focus on results using the base case.

4.2. Modeled CO_2 Fire Emissions Comparison

CT2017 and CT-NRT.v2019-2 simulated fire emissions were subsampled along the ACT-America flight track at 5 s intervals from the 27 km^2 and 3 h resolution pixels and for flight legs below 1 km AGL, then averaged seasonally and by region (Figure 6b). The largest modeled fire contribution in the Mid-Atlantic region was during summer at 10 ± 5 mol CO_2/km^2*h, with other seasons averaging less than 1/3 the fire emissions of summer. Midwestern modeled fire average contributions were highest in spring at ~7.5 ± 3.8 mol CO_2/km^2*h, with emissions in other seasons weaker by an order of magnitude. The Southern region had the highest overall average fire emissions during the fall, winter, and spring seasons, ranging near 20 ± 10 mol CO_2/km^2*h, with a strong drop during summer to ~6 ± 3 mol CO_2/km^2*h.

As the airborne $\Delta CO/\Delta CO_2$ analysis yielded relative CO_2 contributions from BB compared to overall combustion, the magnitude of these emissions cannot be directly compared to the modeled fire contribution. This can be mitigated by normalizing the fire product by the expected FF emissions in each region. Figure 6c shows the same average modeled fire CO_2 emissions as in Figure 6b but normalized by the average 2015 Vulcan modeled total FF CO_2 emissions in each region and season in order to account for the sector variability in overall FF emission. In the same fashion as the simulated fire emissions, data from each sector in the Vulcan inventory (Gurney et al., 2020b) were subsampled to 27 km^2 resolution pixels and interpolated at 5 s intervals along ACT-America flight tracks below 1 km AGL. As seen comparing Figures 6b and 6c, the effect of the FF-normalization did not qualitatively change the trends observed in the fire product averages. This minimal effect combined with the low variability in annual total US FF CO_2 emissions estimated by Vulcan between 2010 and 2015 (99%–106% of 2015

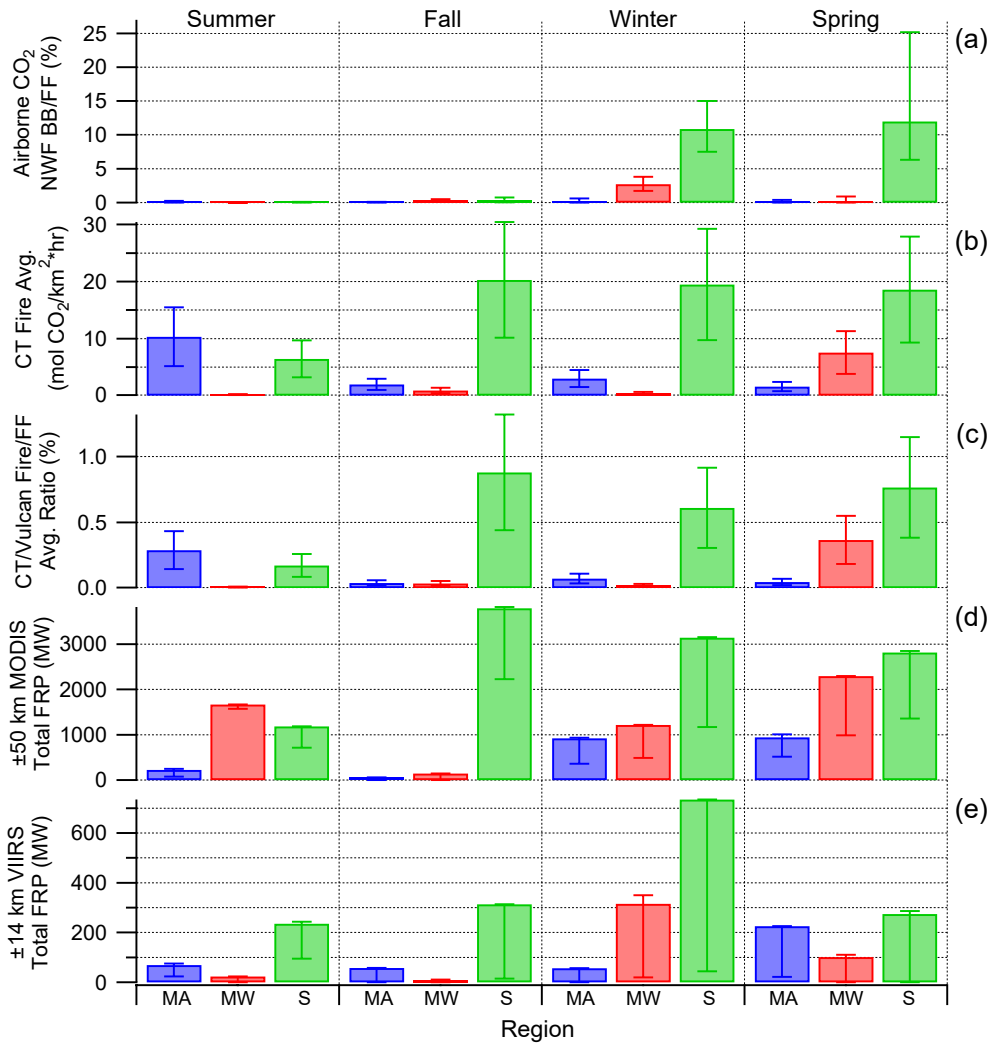

Figure 6. (a) Ratio of NWF contributions from BB/FF from base case airborne analysis by region and season in PBL (<1 km AGL). Error bars denote range in variability from sensitivity analysis. (b) CT2017 & CT-NRT.v2019-2 27 km^2 modeled fire emissions along aircraft flight track. (c) Ratio of modeled fire emissions to Vulcan FF emissions along flight track. (d) Total MODIS 1 km FRP within 50 km of flight track at <1 km AGL altitude at nominal or better confidence. Upper error bars denote low or better confidence and lower error bars denote only high confidence. (e) Total VIIRS 375 m FRP within 14 km of flight track at <1 km AGL altitude separated by season and region at nominal or better confidence. Upper error bars denote low or better confidence and lower error bars denote only high confidence.

emissions; Gurney et al., 2020b) supports the validity of applying the 2015 CO_2 emissions during our 2016–2018 campaign years.

The FF-normalized modeled fire emission ratios (Fire/FF) are directly comparable to the airborne BB/FF ratios. Seasonal and regional trends in the normalized Fire/FF ratios were very similar to those that form the fire product. Figure 6a shows the base case results of the sensitivity analysis described in Section 4.1. The airborne BB/FF ratio values were <0.5% for all regions during summer and fall. Comparably high BB/FF ratios were observed in the South during winter and spring, low ratios were observed in the Mid-Atlantic region in both seasons and the Midwestern spring, whereas Midwestern winter ratios were between the two scenarios. The modeled Fire/FF ratios captured the high airborne BB/FF ratios during winter and spring in the South compared to other regions, with a modeled Fire/FF winter to spring ratio of 1.05 ± 0.74 compared to an airborne FF/BB of $1.07^{+0.75}_{-0.66}$. However, there are three major discrepancies to highlight. The largest discrepancy is the low Fire/FF emission ratio predicted by the model in the South during fall. The modeled winter to fall Fire/FF ratio in the South was $\sim 1.4 \pm 1.0$, while the equivalent airborne winter to fall fire ratio was much higher at 47^{+296}_{-35}. Another strong discrepancy was

the relative winter to spring ratio in the Midwest, as the modeled Fire/FF spring to winter ratio was 17 ± 12 while the opposite was true for the airborne data, with a BB/FF spring to winter emission ratio of $0.11^{+0.27}_{-0.11}$ due to the relative lack of observed fire emissions in the spring. The final major discrepancy was the marked abundance of modeled emissions in the summer in both the Mid-Atlantic and Southern regions, as the airborne BB/FF ratios were negligible during that season in all three regions.

4.3. MODIS and VIIRS Fire Data

As the modeled fire product is parameterized using MODIS 1° fire counts (Jacobson et al., 2020), examining trends in satellite fire count could help understand the differences between the modeled results and aircraft observations. MODIS 1 km (FIRMS, 2020a) and VIIRS-SNPP 375 m (FIRMS, 2020b) fire radiative power (FRP), a measure of the irradiative intensity of the fire, was analyzed over each ACT-America campaign season and region. FRP is used by models to determine the amount of combusted organic matter, and thus should scale with CO_2 emission (Kaiser et al., 2012). Data were filtered for flight days and aircraft altitudes below 1 km AGL. For MODIS, data were filtered for fires detected within 50 km (~±0.5°) of the aircraft flight tracks, the same resolution as the MODIS product used to drive the fire emissions. For VIIRS, data were filtered for fires detected within 14 km of the aircraft flight tracks, comparable to the 27 km^2 resolution of the modeled data. Figures 6d and 6e summarize the FRP-weighted sum of fire counts from each instrument by season and region for MODIS and VIIRS, respectively, while Figures S12 and S13 in Supporting Information S1 show the full spatial distribution of the fire counts and FRP. This is a much-simplified approach to methods described in the literature used to translate FRP to gas emissions but is applied here as a tool to provide insight into the model/airborne agreement. Broadly, the MODIS fire products agreed well with the fire product (Figure 6b). The highest number of fire counts were in the South for all seasons, and there were many fewer counts in the South during summer compared to the other seasons, both matching the modeled fire emissions. This is consistent with Zhang et al. (2010), who found strong correlations in the southeastern US between levoglucosan concentrations, a biomass burning tracer and MODIS fire counts for all seasons except December and January. This discrepancy was hypothesized to be due to the increased occurrence of small-scale residential burning undetectable by MODIS. One of the biggest discrepancies between MODIS and the modeled fire emissions was during summer. While the modeled fire emissions were highest in the Mid-Atlantic region during summer, the MODIS weighted counts were lowest in the Mid-Atlantic. Additionally, the modeled fire emissions in the Midwest during winter were a factor of ~7 smaller compared to those from the Mid-Atlantic region, and the two regions had comparable MODIS weighted counts. The causes for this may be attributable to differences in the very simple FRP weighting approach used here and the more complex analysis performed by the GFED and CASA modules.

Results using the VIIRS weighted counts were significantly different from MODIS. The ratio of Southern spring to winter weighted counts was ~90% from MODIS compared to ~40% from VIIRS, and the ratio of Southern fall to winter weighted counts dropped from ~115% from MODIS to ~45% from VIIRS. Additionally, the ratio of winter to spring weighted counts in the Midwest increased from ~55% with MODIS to ~300% with VIIRS. As two of the largest discrepancies between the modeled and airborne emissions were the modeled high emissions in the South during fall and the ratio of winter to spring emissions in the Midwest, these shifts provide some circumstantial evidence that spatial resolution of either the satellite product or model may be contributing to those discrepancies. Given the uncertainty in the exact range of sensitivity of the airborne NWF method, it is possible as well that the 14 and 50 km cutoffs were too small. Figures S14 and S15 in Supporting Information S1 show a sensitivity analysis looking at total FRP from MODIS and VIIRS, respectively. While these larger scales do result in higher relative total FRP in the Southern region across all seasons, they still fail to reproduce the much-reduced level of fire activity during fall observed in the airborne FF/BB ratios.

5. Conclusions

In this study, we used airborne measurements conducted during the ACT-America campaigns of CO and CO_2 in the PBL to examine the relative frequency of regional and seasonal CO_2 enhancements as a function of $\Delta CO/\Delta CO_2$ enhancement ratio, used as a proxy for CE, over central and eastern US through weighted sliding correlations. Observed enhancement ratios were separated into three regimes: biomass burning (BB), fossil fuel (FF) combustion, and those with apparent negatively sloped (NS) enhancement ratios. Contributions from the NS regime were high in the summer, complicating the analysis. However, sensitivity analyses with the seemingly

biosphere-related NS regime show that the trends in the normalized BB/FF contributions were not strongly affected by this interference. Based on the airborne observations, PBL CO_2 BB emission contributions ($\Delta CO/\Delta CO_2 >$ 4%) relative to FF were seen to be strongest in South in winter and spring, with Mid-Atlantic BB contributions very low or negligible for all seasons. Modeled CO_2 Fire/FF emissions were calculated using modeled fire CO_2 emissions from NOAA's CarbonTracker, versions CT2017 and CT-NRT-v2019-2 and modeled FF CO_2 emissions from the Vulcan v3.0 2015 inventory. These modeled CO_2 Fire/FF emissions agreed with these high relative fire emissions in the South, but also predicted enhanced Fire/FF emissions in the South during fall, in the Midwest during spring, and in the Mid-Atlantic region in the summer. Analysis of FRP-weighted satellite showed that while the 1 km MODIS fire data more accurately reproduced the modeled fire emissions, the 375 m VIIRS fire data reduced the overpredictions during the Southern fall and Midwestern spring. This suggests that the spatial resolution of the satellite products driving the model affects the measurement/model discrepancy, though does not explain the discrepancy in the Mid-Atlantic summer. These results imply that a combination of factors, such as undetected smaller agricultural fires below satellite product resolution or insufficiently constrained biosphere data, may cause significant biases in predictions of BB CO_2 emissions in the US. Additionally, as air quality models use similar modules to drive BB VOC and CO emissions, these same biases would likely affect predictions of regional air quality as well.

Data Availability Statement

We acknowledge the use of data from the NASA FIRMS application (https://firms.modaps.eosdis.nasa.gov/) operated by the NASA Goddard Space Flight Center Earth Science Data and Information System (ESDIS) project. All data are available from publicly accessible archives: https://doi.org/10.3334/ORNLDAAC/1593 (aircraft), https://doi.org/10.25925/V3K6-5168 (CT2017), https://gml.noaa.gov/ccgg/carbontracker/CT-NRT.v2019-2/ (CT-NRT.v2019-2), and https://doi.org/10.3334/ORNLDAAC/1741 (Vulcan).

Acknowledgments
The Atmospheric Carbon and Transport (ACT)-America project is a NASA Earth Venture Suborbital-2 project funded by NASA's Earth Science Division (Grant NNX15AG76G to Penn State). Co-author SP was supported by NASA Grant Number 80NSSC19K0730 and Texas Tech University. We would like to thank James Plant, James Geiger, and Ali Aknan for their assistance with in situ instrument payload preparation and data collection. Thanks to Michael Obland, Byron Meadows, and Bing Lin for mission support and coordination. Thanks to Jocelyn Turnbull for helpful suggestions throughout the review process. Thanks to NASA Wallops Flight Facility and NASA Langley Research Center for aircraft operations and logistics support. Thanks to Melissa Yang and BAER/NSRC for aircraft navigational and meteorological data support. Thanks to Duncan Aviation and TAC Air for FBO and logistics support during the ACT-America campaigns. CarbonTracker CT2017 and CT-NRT.v2019-2 results provided by NOAA ESRL, Boulder, Colorado, USA from the website at http://carbontracker.noaa.gov.

References

Akagi, S. K., Yokelson, R. J., Wiedinmyer, C., Alvarado, M. J., Reid, J. S., Karl, T., et al. (2011). Emission factors for open and domestic biomass burning for use in atmospheric models. *Atmospheric Chemistry and Physics*, *11*(9), 4039–4072. https://doi.org/10.5194/acp-11-4039-2011

Andreae, M. O., & Merlet, P. (2001). Emission of trace gases and aerosols from biomass burning. *Global Biogeochemical Cycles*, *15*(4), 955–966. https://doi.org/10.1029/2000GB001382

Andrew, R. M. (2018). Global CO_2 emissions from cement production. *Earth System Science Data*, *10*(1), 195–217. https://doi.org/10.5194/essd-10-195-2018

Baier, B. C., Sweeney, C., Choi, Y., Davis, K. J., DiGangi, J. P., Feng, S., et al. (2020). Multispecies assessment of factors influencing regional and enhancements during the winter 2017 ACT-America Campaign. *Journal of Geophysical Research: Atmospheres*, *125*(2), e2019JD031339. https://doi.org/10.1029/2019JD031339

Bell, E., O'Dell, C. W., Davis, K. J., Campbell, J., Browell, E., Denning, A. S., et al. (2020). Evaluation of OCO-2 X_{CO2} variability at local and synoptic scales using Lidar and in situ observations from the ACT-America Campaigns. *Journal of Geophysical Research: Atmospheres*, *125*(10), e2019JD031400. https://doi.org/10.1029/2019JD031400

Campbell, J. F., Lin, B., Dobler, J., Pal, S., Davis, K., Obland, M. D., et al. (2020). Field evaluation of column CO_2 retrievals from intensity-modulated continuous-wave differential absorption lidar measurements during the ACT-America Campaign. *Earth and Space Science*, *7*(12), e2019EA000847. https://doi.org/10.1029/2019EA000847

CarbonTracker Team. (2018). *CarbonTracker CT2017*. NOAA Earth System Research Laboratory, Global Monitoring Division. https://doi.org/10.25925/V3K6-5168

Cui, Y. Y., Jacobson, A. R., Feng, S., Wesloh, D., Barkley, Z. R., Zhang, L., et al. (2021). Evaluation of CarbonTracker's inverse estimates of North American net ecosystem exchange of CO_2 from different observing systems using ACT-America airborne observations. *Journal of Geophysical Research: Atmospheres*, *126*, e2020JD034406. https://doi.org/10.1029/2020JD034406

Davis, K. J., Browell, E. V., Feng, S., Lauvaux, T., Obland, M. D., Pal, S., et al. (2021). The atmospheric carbon and transport (ACT) – America Mission. *Bulletin of the American Meteorological Society*, *102*(9), E1714–E1734. https://doi.org/10.1175/BAMS-D-20-0300.1

Davis, K. J., Obland, M. D., Lin, B., Lauvaux, T., O'dell, C., Meadows, B., et al. (2018). ACT-America: L3 merged in situ atmospheric trace gases and flask data, Eastern USA. *ORNL DAAC*. https://doi.org/10.3334/ORNLDAAC/1593

Djuricin, S., Pataki, D. E., & Xu, X. (2010). A comparison of tracer methods for quantifying CO_2 sources in an urban region. *Journal of Geophysical Research*, *115*(D11). https://doi.org/10.1029/2009JD012236

Dlugokencky, E. J., Myers, R. C., Lang, P. M., Masarie, K. A., Crotwell, A. M., Thoning, K. W., et al. (2005). Conversion of NOAA atmospheric dry air CH_4 mole fractions to a gravimetrically prepared standard scale. *Journal of Geophysical Research*, *110*(D18). https://doi.org/10.1029/2005JD006035

Eldering, A., Wennberg, P. O., Crisp, D., Schimel, D. S., Gunson, M. R., Chatterjee, A., et al. (2017). The orbiting carbon observatory-2 early science investigations of regional carbon dioxide fluxes. *Science*, *358*(6360). https://doi.org/10.1126/science.aam5745

FIRMS. (2020a). *MODIS/Aqua+Terra thermal anomalies/fire locations 1km FIRMS V006*. https://doi.org/10.5067/FIRMS/MODIS/MCD14ML

FIRMS. (2020b). *VIIRS (S-NPP) I Band 375 m active fire product NRT (Vector data)*. https://doi.org/10.5067/FIRMS/VIIRS/VNP14IMGT_NRT.002

Fyfe, J. C., Kharin, V. V., Swart, N., Flato, G. M., Sigmond, M., & Gillett, N. P. (2021). Quantifying the influence of short-term emission reductions on climate. *Science Advances*, *7*(10), eabf7133. https://doi.org/10.1126/sciadv.abf7133

Giglio, L., Randerson, J. T., & van der Werf, G. R. (2013). Analysis of daily, monthly, and annual burned area using the fourth-generation global fire emissions database (GFED4). *Journal of Geophysical Research: Biogeosciences*, *118*(1), 317–328. https://doi.org/10.1002/jgrg.20042

Gonzalez, A., Millet, D. B., Yu, X., Wells, K. C., Griffis, T. J., Baier, B. C., et al. (2021). Fossil versus nonfossil CO sources in the US: New airborne constraints from ACT-America and GEM. *Geophysical Research Letters*, *48*(11), e2021GL093361. https://doi.org/10.1029/2021GL093361

Graven, H. D., Stephens, B. B., Guilderson, T. P., Campos, T. L., Schimel, D. S., Campbell, J. E., et al. (2009). Vertical profiles of biospheric and fossil fuel-derived CO_2 and fossil fuel CO_2:CO ratios from airborne measurements of Δ14C, CO_2 and CO above Colorado, USA. *Tellus B: Chemical and Physical Meteorology*, *61*(3), 536–546. https://doi.org/10.1111/j.1600-0889.2009.00421.x

Gregory, J. M., Jones, C. D., Cadule, P., & Friedlingstein, P. (2009). Quantifying carbon cycle feedbacks. *Journal of Climate*, *22*(19), 5232–5250. https://doi.org/10.1175/2009JCLI2949.1

Griffin, R. J., Chen, J., Carmody, K., Vutukuru, S., & Dabdub, D. (2007). Contribution of gas phase oxidation of volatile organic compounds to atmospheric carbon monoxide levels in two areas of the United States. *Journal of Geophysical Research*, *112*(D10). https://doi.org/10.1029/2006JD007602

Gurney, K. R., Liang, J., Patarasuk, R., Song, Y., Huang, J., & Roest, G. (2020a). The vulcan version 3.0 high-resolution fossil fuel CO_2 emissions for the United States. *Journal of Geophysical Research: Atmospheres*, *125*(19), e2020JD032974. https://doi.org/10.1029/2020JD032974

Gurney, K. R., Liang, J., Patarasuk, R., Song, Y., Huang, J., & Roest, G. (2020b). Vulcan: High-Resolution annual fossil fuel CO_2 emissions in USA, 2010-2015, version 3. *ORNL DAAC* https://doi.org/10.3334/ORNLDAAC/1741

Halliday, H. S., DiGangi, J. P., Choi, Y., Diskin, G. S., Pusede, S. E., Rana, M., et al. (2019). Using short-term CO/CO_2 ratios to assess air mass differences over the Korean Peninsula during KORUS-AQ. *Journal of Geophysical Research: Atmospheres*, *124*(20), 10951–10972. https://doi.org/10.1029/2018JD029697

Hannun, R. A., Wolfe, G. M., Kawa, S. R., Hanisco, T. F., Newman, P. A., Alfieri, J. G., et al. (2020). Spatial heterogeneity in CO2, CH4, and energy fluxes: Insights from airborne eddy covariance measurements over the Mid-Atlantic region. *Environmental Research Letters*, *15*(3), 035008. https://doi.org/10.1088/1748-9326/ab7391

Holloway, T., Levy, H., & Kasibhatla, P. (2000). Global distribution of carbon monoxide. *Journal of Geophysical Research: Atmospheres*, *105*(D10), 12123–12147. https://doi.org/10.1029/1999JD901173

Jacobson, A. R., Schuldt, K. N., Miller, J. B., Oda, T., Tans, P., Andrews, A., et al. (2020). *CarbonTracker CT2019*. https://doi.org/10.25925/39M3-6069

Jung, M., Reichstein, M., Margolis, H. A., Cescatti, A., Richardson, A. D., Arain, M. A., et al. (2011). Global patterns of land-atmosphere fluxes of carbon dioxide, latent heat, and sensible heat derived from eddy covariance, satellite, and meteorological observations. *Journal of Geophysical Research: Biogeosciences*, *116*(G3). https://doi.org/10.1029/2010JG001566

Kaiser, J. W., Heil, A., Andreae, M. O., Benedetti, A., Chubarova, N., Jones, L., et al. (2012). Biomass burning emissions estimated with a global fire assimilation system based on observed fire radiative power. *Biogeosciences*, *9*(1), 527–554. https://doi.org/10.5194/bg-9-527-2012

Kostinek, J., Roiger, A., Davis, K. J., Sweeney, C., DiGangi, J. P., Choi, Y., et al. (2019). Adaptation and performance assessment of a quantum and interband cascade laser spectrometer for simultaneous airborne in situ observation of CH_4, C_2H_6, CO_2, CO and N_2O. *Atmospheric Measurement Techniques*, *12*(3), 1767–1783. https://doi.org/10.5194/amt-12-1767-2019

LaFranchi, B. W., Pétron, G., Miller, J. B., Lehman, S. J., Andrews, A. E., Dlugokencky, E. J., et al. (2013). Constraints on emissions of carbon monoxide, methane, and a suite of hydrocarbons in the Colorado Front Range using observations of $^{14}CO_2$. *Atmospheric Chemistry and Physics*, *13*(21), 11101–11120. https://doi.org/10.5194/acp-13-11101-2013

Lauvaux, T., Schuh, A. E., Uliasz, M., Richardson, S., Miles, N., Andrews, A. E., et al. (2012). Constraining the CO_2 budget of the corn belt: Exploring uncertainties from the assumptions in a mesoscale inverse system. *Atmospheric Chemistry and Physics*, *12*(1), 337–354. https://doi.org/10.5194/acp-12-337-2012

Middlebrook, A. M., Murphy, D. M., Ahmadov, R., Atlas, E. L., Bahreini, R., Blake, D. R., et al. (2012). Air quality implications of the deepwater horizon oil spill. *Proceedings of the National Academy of Sciences*, *109*(50), 20280–20285. https://doi.org/10.1073/pnas.1110052108

Novelli, P. C., Elkins, J. W., & Steele, L. P. (1991). The development and evaluation of a gravimetric reference scale for measurements of atmospheric carbon monoxide. *Journal of Geophysical Research: Atmospheres*, *96*(D7), 13109–13121. https://doi.org/10.1029/91JD01108

Pal, S., Davis, K. J., Lauvaux, T., Browell, E. V., Gaudet, B. J., Stauffer, D. R., et al. (2020). Observations of greenhouse gas changes across summer frontal boundaries in the Eastern United States. *Journal of Geophysical Research: Atmospheres*, *125*(5), e2019JD030526. https://doi.org/10.1029/2019JD030526

Peischl, J., Ryerson, T. B., Holloway, J. S., Parrish, D. D., Trainer, M., Frost, G. J., et al. (2010). A top-down analysis of emissions from selected Texas power plants during TexAQS 2000 and 2006. *Journal of Geophysical Research: Atmospheres*, *115*(D16). https://doi.org/10.1029/2009JD013527

Peters, W., Jacobson, A. R., Sweeney, C., Andrews, A. E., Conway, T. J., Masarie, K., et al. (2007). An atmospheric perspective on North American carbon dioxide exchange: CarbonTracker. *Proceedings of the National Academy of Sciences*, *104*(48), 18925–18930. https://doi.org/10.1073/pnas.0708986104

Reum, F., Gerbig, C., Lavric, J. V., Rella, C. W., & Göckede, M. (2019). Correcting atmospheric CO_2 and CH_4 mole fractions obtained with Picarro analyzers for sensitivity of cavity pressure to water vapor. *Atmospheric Measurement Techniques*, *12*(2), 1013–1027. https://doi.org/10.5194/amt-12-1013-2019

Silva, S. J., Arellano, A. F., & Worden, H. M. (2013). Toward anthropogenic combustion emission constraints from space-based analysis of urban CO_2/CO sensitivity. *Geophysical Research Letters*, *40*(18), 4971–4976. https://doi.org/10.1002/grl.50954

Smith, M. L., Kort, E. A., Karion, A., Sweeney, C., Herndon, S. C., & Yacovitch, T. I. (2015). Airborne ethane observations in the Barnett Shale: Quantification of ethane flux and attribution of methane emissions. *Environmental Science & Technology*, *49*(13), 8158–8166. https://doi.org/10.1021/acs.est.5b00219

Sun, Y., Frankenberg, C., Jung, M., Joiner, J., Guanter, L., Köhler, P., et al. (2018). Overview of solar-induced chlorophyll fluorescence (SIF) from the orbiting carbon observatory-2: Retrieval, cross-mission comparison, and global monitoring for GPP. *Remote Sensing of Environment*, *209*, 808–823. https://doi.org/10.1016/j.rse.2018.02.016

Suntharalingam, P., Jacob, D. J., Palmer, P. I., Logan, J. A., Yantosca, R. M., Xiao, Y., et al. (2004). Improved quantification of Chinese carbon fluxes using CO_2/CO correlations in Asian outflow. *Journal of Geophysical Research: Atmospheres*, *109*(D18). https://doi.org/10.1029/2003jd004362

Tans, P. P., Crotwell, A. M., & Thoning, K. W. (2017). Abundances of isotopologues and calibration of CO_2 greenhouse gas measurements. *Atmospheric Measurement Techniques*, *10*(7), 2669–2685. https://doi.org/10.5194/amt-10-2669-2017

Turnbull, J. C., Karion, A., Fischer, M. L., Faloona, I., Guilderson, T., Lehman, S. J., et al. (2011). Assessment of fossil fuel carbon dioxide and other anthropogenic trace gas emissions from airborne measurements over Sacramento, California in spring 2009. *Atmospheric Chemistry and Physics*, *11*(2), 705–721. https://doi.org/10.5194/acp-11-705-2011

Turnbull, J. C., Sweeney, C., Karion, A., Newberger, T., Lehman, S. J., Tans, P. P., et al. (2015). Toward quantification and source sector identification of fossil fuel CO_2 emissions from an urban area: Results from the INFLUX experiment. *Journal of Geophysical Research: Atmospheres*, *120*(1), 292–312. https://doi.org/10.1002/2014JD022555

USEPA. (2010). *AP 42 fifth edition compilation of air pollutant emissions factors. Stationary point and area sources* (Vol. 1). USEPA (United States Environmental Protection Agency).

van der Werf, G. R., Randerson, J. T., Giglio, L., van Leeuwen, T. T., Chen, Y., Rogers, B. M., et al. (2017). Global fire emissions estimates during 1997–2016. *Earth System Science Data*, *9*(2), 697–720. https://doi.org/10.5194/essd-9-697-2017

Venkataraman, C., & Rao, G. U. M. (2001). Emission factors of carbon monoxide and size-resolved aerosols from biofuel combustion. *Environmental Science & Technology*, *35*(10), 2100–2107. https://doi.org/10.1021/es001603d

Wang, J. S., Kawa, S. R., Collatz, G. J., Sasakawa, M., Gatti, L. V., Machida, T., et al. (2018). A global synthesis inversion analysis of recent variability in CO_2 fluxes using GOSAT and in situ observations. *Atmospheric Chemistry and Physics*, *18*(15), 11097–11124. https://doi.org/10.5194/acp-18-11097-2018

Wei, Y., Shrestha, R., Pal, S., Gerken, T., Feng, S., McNelis, J., et al. (2021). Atmospheric carbon and transport – America (ACT-America) Data Sets: Description, management, and delivery. *Earth and Space Science*, *8*(7), e2020EA001634. https://doi.org/10.1029/2020EA001634

Weibring, P., Richter, D., Walega, J. G., Fried, A., DiGangi, J., Halliday, H., et al. (2020). Autonomous airborne Mid-IR spectrometer for high precision measurements of ethane during the NASA ACT-America Studies. *Atmospheric Measurement Techniques Discussions*, 1–42. https://doi.org/10.5194/amt-2020-210

Wu, C., & Yu, J. Z. (2018). Evaluation of linear regression techniques for atmospheric applications: The importance of appropriate weighting. *Atmospheric Measurement Techniques*, *11*(2), 1233–1250. https://doi.org/10.5194/amt-11-1233-2018

Yokota, T., Yoshida, Y., Eguchi, N., Ota, Y., Tanaka, T., Watanabe, H., et al. (2009). Global concentrations of CO_2 and CH_4 retrieved from GOSAT: First preliminary results. *Scientific Online Letters on the Atmosphere*, *5*(1), 160–163. https://doi.org/10.2151/sola.2009-041

Zhang, X., Hecobian, A., Zheng, M., Frank, N. H., & Weber, R. J. (2010). Biomass burning impact on $PM_{2.5}$ over the southeastern US during 2007: Integrating chemically speciated FRM filter measurements, MODIS fire counts and PMF analysis. *Atmospheric Chemistry and Physics*, *10*(14), 6839–6853. https://doi.org/10.5194/acp-10-6839-2010